IEEE Access
Multidisciplinary ⋮ Rapid Review ⋮ Open Access Journal

Received January 27, 2021, accepted February 22, 2021, date of publication March 15, 2021, date of current version March 26, 2021.

Digital Object Identifier 10.1109/ACCESS.2021.3065968

Image Dehazing in Disproportionate Haze Distributions

SHIH-CHIA HUANG[1], **(Senior Member, IEEE), DA-WEI JAW**[2], **WENLI LI**[3], **ZHIHUI LU**[4,5], **(Member, IEEE), SY-YEN KUO**[2], **(Fellow, IEEE), BENJAMIN C. M. FUNG**[6], **(Senior Member, IEEE), BO-HAO CHEN**[7,8], **(Member, IEEE), AND THANISA NUMNONDA**[9]

[1]Department of Electronic Engineering, National Taipei University of Technology, Taipei 10608, Taiwan
[2]Department of Electrical Engineering, National Taiwan University, Taipei 10617, Taiwan
[3]Educational Technology and Information Center, Shenzhen Polytechnic, Shenzhen 518055, China
[4]School of Computer Science, Fudan University, Shanghai 200433, China
[5]Engineering Research Center of Cyber Security Auditing and Monitoring, Ministry of Education, Shanghai 200433, China
[6]School of Information Studies, McGill University, Montreal, QC H3A 1X1, Canada
[7]Department of Computer Science and Engineering, Yuan Ze University, Taoyuan 32003, Taiwan
[8]Innovation Center for Big Data and Digital Convergence, Yuan Ze University, Taoyuan 32003, Taiwan
[9]Faculty of Information Technology, King Mongkut's Institute of Technology Ladkrabang, Bangkok 10520, Thailand

Corresponding authors: Wenli Li (lwlszpt@163.com) and Thanisa Numnonda (thanisa@it.kmitl.ac.th)

This work was supported in part by the National Taipei University of Technology through the NTUT-KMITL Joint Research Program under Grant NTUT-KMITL-106-03, and in part by the Shanghai 2018 Innovation Action Plan Project under Grant 18510760200.

ABSTRACT Haze removal techniques employed to increase the visibility level of an image play an important role in many vision-based systems. Several traditional dark channel prior-based methods have been proposed to remove haze formation and thereby enhance the robustness of these systems. However, when the captured images contain disproportionate haze distributions, these methods usually fail to attain effective restoration in the restored image. Specifically, disproportionate haze distribution in an image means that the background region possesses heavy haze density and the foreground region possesses little haze density. This phenomenon usually occurs in a hazy image with a deep depth of field. In response, a novel hybrid transmission map-based haze removal method that specifically targets this situation is proposed in this work to achieve clear visibility restoration and effective information maintenance. Experimental results via both qualitative and quantitative evaluations demonstrate that the proposed method is capable of performing with higher efficacy when compared with other state-of-the-art methods, in respect to both background regions and foreground regions of restored test images captured in real-world environments.

INDEX TERMS Haze removal, disproportionate haze distribution, dark channel prior.

I. INTRODUCTION

Among the predominant causes of low-visibility in digital image acquisition is the absorption and scattering of light by large amounts of turbid medium via atmospheric movements. However, in many vision-based applications such as surveillance systems [1]–[5], intelligent transportation systems [6], or face annotation systems [7], often only a few objects can be featured in video camera footage due to low-visibility constraints such as haze, fog, and mist. The primary aim of a haze removal technique is to increase the visibility level of an image while recovering object information, thereby enhancing the performance of these vision-based applications.

The associate editor coordinating the review of this manuscript and approving it for publication was Mehul S. Raval.

Haze removal techniques can be separated into two major groups depending on the data type it process, one are those non-single image information techniques [8]–[13], and the other one are those single image information techniques [14]–[23]. Among the two groups, removing haze from single image shows more challenging due to the lack of multiple data sources or temporal information.

In the literature of single image information based methods, there exist two major categories: the data-driven methods that utilized machine learning techniques to learn the mapping between hazy image and either the corresponding haze-free image or the transmission map [16]–[20], [24]. However, although learning-based method can achieve fine results on images with even haze distributions, it often suffers from failure recovery when it comes to those images with disproportionate haze distributions. The reasons behind such failure are that, under the assumption of haze particles are evenly distributed within an image, the design of neural networks often consists of multiple mean-pooling layers, and the utilization of synthesized hazy images also lacks the consideration on the disproportionate haze distribution problem. This design leads to a relatively smoothed estimation of haze distribution, thereby failed on the recovery of those disproportionate haze.

On the other hand, approaches in the second category designed hand-crafted priors to recover the hazy image show good results and generalization ability [14], [21], [25]–[34]. Fattal [25] proposed a haze removal method that is based on an independent component analysis by assuming that the transmission and surface shading are uncorrelated to estimate the transmission map and further recover the visibility of a hazy image. Tan's method [26] restored hazy images by both maximizing the local contrast and constraining the intensity of each pixel to be less than the intensity of global atmospheric light. He *et al.* [14] developed a haze removal method primarily based on an assumption that there is at least one pixel possessing low intensity that exists within a local patch in outdoor haze-free images outside of sky regions. In Bui *et al.*'s work [21], they constructed a statistical color ellipsoid prior as well as utilized a fuzzy segmentation process to simultaneously estimates the transmission and executes the refinement process to efficiently enhance the hazy image.

Among the prior-based approaches, the specific dark channel prior-based methods [14], [27]–[31] are very efficient for visibility restoration. He *et al.* proposed the dark channel prior assumption to estimate haze thickness [14]. This assumption is based on the key observation that an outdoor haze-free image without a sky region possesses at least one pixel of lower intensity between the RGB color channels. The approach of Wang and Wu [27] adopted the dark channel prior and the soft matting technique to estimate the haze thickness and refine the transmission map. Eventually, the haze-free image can be attained based on the use of its restoration function. The dark channel prior was refined by the approach of Ullah *et al.* [28]. in which the dark channel of the incoming hazy image was initially produced in the HSI color space. Then, the soft matting technique was also employed to refine the transmission map, and the haze-free image was therefore attained. Xu *et al.*'s method [29] employed He *et al.*'s transmission estimation function [14] to produce the haze thickness of the incoming hazy image in the transmission map, and additionally utilized the fast bilateral filter to refine the transmission map instead of the soft matting technique. Moreover, Xu *et al.* employ a threshold setting to determine whether or not the restoration process is necessary for the restoration function to further improves the efficiency. In Gao *et al.*'s work [30], they firstly proposed to use two priors, namely, depth-edge aware prior and airlight impact regularity prior, and an airlight refinement algorithm to refine the dark channel. Secondly, an adaptive sharpening model for eliminating the airlight additive influence as well as the convolution effects is utilized to enhance the image details. Hu *et al.*'s method [31] proposes to improve the atmospheric scattering model via adaptively compensate the illumination intensity and using joint local-global illumination adjustment to accomplish haze removal.

However, these dark channel prior-based methods often fail to restore hazy images that have disproportionate haze distributions. This is due to the haze density cannot be effectively estimated in the transmission map by using the dark channel prior with only a single patch-size for the images. To overcome this problem, we propose a novel hybrid transmission map-based haze removal algorithm using the existing dark channel prior. The proposed method specifically targets the hazy images that contain disproportionate haze distributions. These images usually contain heavy haze formation in their background regions and little haze formation in their foreground regions. Since the proposed algorithm lies within this scope of dark channel prior strategies, we discuss hereafter the most commonly used dark channel prior-based techniques that have been considered effective for haze-density estimation.

II. BACKGROUND

In general, observed light is irregularly absorbed and scattered by atmosphere-turbid media (e.g., haze) in poor weather conditions. An observation model was therefore proposed in previous works to represent the formation of a hazy image according to this atmospheric phenomenon [33]. For each incoming pixel, the observation model can be expressed as follows:

$$I(x) = J(x)\, t(x) + A(1 - t(x)) \tag{1}$$

where x represents each pixel position of the hazy image I, the haze-free image J, and the transmission map t, respectively; A represents the global atmospheric light. Inspired by this model, investigations of the dark channel prior-based approaches [14], [27]–[29] have been proposed to enhance the visibility of hazy images captured during poor weather conditions. A detailed survey of these investigations is presented below.

According to the dark channel prior assumption, He *et al.* adopts a minimum filter to estimate the transmission map $\tilde{t}$ of the hazy image, which can be regarded as haze thickness, in order to restore the visibility of hazy images [14]. Hence, the transmission map $\tilde{t}_{p_{15\times15}}$ can be obtained by:

$$\tilde{t}_{p_{15\times15}}(x) = 1 - \omega \min_{y\in p_{15\times15}(x)} \left\{ \min_{c\in\{r,g,b\}} \frac{I_c(y)}{A_c} \right\} \tag{2}$$

where $c \in \{r, g, b\}$, $p_{15\times15}(x)$ represents a local patch centered at position x, y is the corresponding pixel within the local patch $p_{15\times15}(x)$, and $\min_{c\in\{r,g,b\}}$ represents the minimum filter that is used to pick up the minimum value of the pixel from the incoming hazy image I_c. Here, the right term for Eq. (2) is a dark channel prior process with an adjusted constant ω, by which to calculate the haze thickness of an incoming hazy image I_c. In addition, the adjusted constant ω can be fixed

FIGURE 1. **Comparison of restoration results produced via the methods of He *et al.*, Gao *et al.* and Hu *et al.*.**

to 0.95, which is suggested by [14] to maintain some haze formation in the restored image. This is because the restored image may look unnatural if its haze formation is entirely removed. In the beginning of the procedure, all pixels of the incoming hazy image are initialized between 0 and 1.

According to [14], the size of a local patch $p_{15\times15}(x)$ experimentally set to 15×15 yields much better results for visibility restoration. However, an image restored via the use of the transmission map $\tilde{t}_{p_{15\times15}}$, which is produced by employing Eq. (2), results in generation of block artifacts. To overcome this problem, He *et al.* adopted the soft matting technique to refine the transmission map $\tilde{t}_{p_{15\times15}}$. Initially, the element (m, n) of the matting Laplacian matrix L is given as

$$\sum_{k|(m,n)\in\omega_k}\left(\delta_{mn}-\frac{1}{|\omega_k|}\left(1+(I_m-\mu_k)^T\left(\sum\nolimits_k\right.\right.\right.$$
$$\left.\left.\left.+\frac{\varepsilon}{|\omega_k|}U_3\right)^{-1}(I_n-\mu_k)\right)\right) \quad (3)$$

where I_m and I_n represent the pixels of the input color image I at position m and n, respectively; μ_k and $\sum_k$ represent the mean matrix and the covariance matrix of the pixels in window ω_k, respectively; δ_{mn} represents Kronecker delta; U_3 represents an identity matrix, the size of which can be set to 3; $|\omega_k|$ represents the number of pixels in the window ω_k. Subsequently, the refined transmission map $t_{p_{15\times15}}$ can be attained from the solution of the sparse linear system, which is obtained as follows:

$$(L+\lambda U)\, t_{p_{15\times15}}=\lambda\tilde{t}_{p_{15\times15}} \quad (4)$$

where L and U represent the Laplacian matrix and the identity matrix with the same size as L, respectively. Note that λ can be set to 10^{-4}, empirically.

As the last step of their approach, He *et al.* adopted the refined transmission map $t_{p_{15\times15}}$ to restore the incoming hazy image I_c as the haze-free image J_c. This restoration function can be expressed as:

$$J_c(x)=\frac{I_c(x)-A_c}{\max\{t_{p_{15\times15}}(x),t_0\}}+A_c \quad (5)$$

where $c \in \{r, g, b\}$, t_0 represents the lower bound of the refined transmission map $t_{p_{15\times15}}$, and A_c represents the global atmospheric light. Note that t_0 is empirically set to 0.1 according to [14]. Moreover, A_c is set to the highest intensity value in each RGB color channel of the incoming hazy image I_c within a region that is extracted from the top 0.1 percent brightest pixels in the dark channel of the incoming hazy image I_c.

A. DISCUSSION

In general, the use of the dark channel prior can effectively estimate haze thickness for ideal hazy images that contain uniform haze distributions (e.g., the background and foreground regions contain proportionate haze formation), as indicated in Fig. 1. However, when the images contain disproportionate haze distributions, such that which occurs in images with deep depths of field, the use of the dark channel prior results in an ineffective estimation of haze thickness in the transmission map produced when using the single patch-size (e.g., 3×3 or 15×15).

For example, He *et al.*'s method [14] employs the dark channel prior to produce a transmission map via a single patch-size (e.g., 3×3 or 15×15) in order to restore a hazy image with disproportionate haze formation, as shown in Fig. 2. Specifically, the red square in Fig. 2 (a) presents the haze-free foreground region in the captured image. As shown in the red square in Fig. 2 (d), the information of the foreground region can be effectively maintained in the restored image produced via the use of the patch-size 15×15. In contrast with the red square in Fig. 2 (d), the red square in Fig. 2 (e) clearly contains artifact effects due to the use of the transmission map produced by using patch-size 3×3. This is because the patch-size 3×3 possesses smaller search regions than the patch-size 15×15. In other words, there is a lower probability of finding the pixel of low intensity in the dark channel when using a patch-size of 3×3. Thus, the haze-free foreground region in the transmission map used when adopting a patch-size of 3×3 is often misjudged as containing haze. For this reason, the haze-free foreground region in the restored image contains artifact effects in the red square in Fig. 2 (e).

In contrast, the blue square in Fig. 2 (a) presents the haze background region in the captured image. As can be observed in the blue square in Fig. 2 (e) and Fig. 2 (d), the visibility of the background region within the image restored by using the single patch-size 15×15 is poorer than the image restored by using the single patch-size 3×3. This is because the haze thickness in the dark channel is estimated by employing the patch-size 15×15, which possesses larger search regions for the extraction of low intensity pixels than the patch-size 3×3 does. For this reason, the haze thickness in the transmission

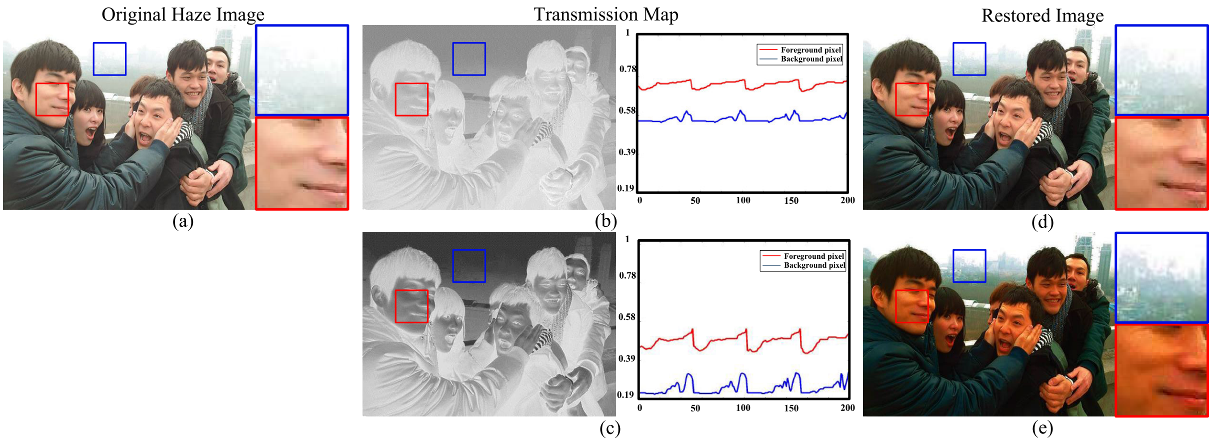

FIGURE 2. Restoration results produced via different single patch-sizes by the dark channel prior method: (a) is the incoming hazy image; (b) and (c) present the transmission map and its corresponding intensity value within regions of background and foreground generated by utilizing a single patch-size of 15 × 15 and 3 × 3, respectively; (d) and (e) show the restored images produced by using the single patch-size of 15 × 15 and 3 × 3, respectively.

map that uses patch-size 15 × 15 is thinner than that is estimated by using the patch-size 3 × 3, thereby reducing the capability of haze removal, as indicated by the blue square and blue waveform in Fig. 2 (c). According to the blue square in Fig. 2 (e) and 2 (d), it is apparent that the visibility of the background region restored by using the patch-size 3 × 3 is more effective than that which is restored via the use of the patch-size 15 × 15 in regard to the deep depth of field of the hazy image.

In order to attain clear visibility restoration within the background region and the maintenance of the intrinsic structure within the foreground region, we combine the advantages of two transmission maps generated by these two single patch-sizes to produce the hybrid transmission map and restore hazy images with disproportionate haze formation.

B. CONTRIBUTIONS

In this paper, we propose a novel haze removal method consisting of the proposed haze thickness estimation (HTE) module and the proposed haze formation removal (HFR) module for hazy images in order to obtain effective restoration results. During the proposed HTE module, we first produce a hybrid transmission map by preserving the strengths of the two types of transmission maps produced by adopting patch-sizes 15 × 15 and 3 × 3. Subsequently, clear visibility restoration and effective information maintenance can be achieved via the use of the hybrid transmission map in the proposed HFR module.

In comparison with the traditional dark channel prior-based methods, the proposed method yields two major contributions:

1) Clear visibility restoration: the proposed method can more sufficiently remove haze formation from real-world hazy images than the traditional dark channel prior-based methods.
2) Effective information maintenance: the proposed method can more effectively preserve the intrinsic structure of a haze-free foreground region in the restored image.

The paper is divided into five main sections. The details of the proposed novel haze removal method are presented in Section III. Section IV presents the experimental results that contrast the proposed method with other state-of-the-art methods by using both qualitative and quantitative analyses. Section V concludes this paper.

III. PROPOSED METHOD

The need and challenges of haze removal techniques were explained in the previous section. To overcome its challenges, we first incorporate the respective strengths of both transmission maps via the use of a saliency map with a Laplacian-pyramids-based merging technique to yield the hybrid transmission map. Next, haze formation can be effectively removed by using the hybrid transmission map.

To this end, we performed a closer investigation and analyzed these two transmission maps, and made the following observations:

1) Haze thickness increases for each transmission map as distance increases between the camera and captured object in the image.
2) As discussed in pervious section, the haze thickness estimated by using a patch-size 3 × 3 is heavier than that estimated by using a patch-size 15 × 15, according to these two transmission maps.
3) For most restored images, the use of each transmission map produces different restoration results for background regions and foreground regions, as shown in Fig. 3. In other words, the restored images rarely show clear visibility restoration while maintaining effective structure for each region.

A. HAZE THICKNESS ESTIMATION

According to these observations, we employed the transmission maps produced with a patch-size of 15 × 15 for restoring

FIGURE 3. Restored images obtained by using each transmission map; the first row shows the original hazy images; the second row shows the images restored by using the transmission map through a patch-size of 3 × 3; the third row shows the images restored by using the transmission map through a patch-size of 15 × 15.

haze-free foreground regions of the images. Accordingly, the first transmission map $\tilde{t}_{p_{15\times15}}$ is based on patch-size 15 × 15 and is given by

$$\tilde{t}_{p_{15\times15}}(x) = 1 - \omega \min_{y\in p_{15\times15}(x)} \left\{ \min_{c\in\{r,g,b\}} \frac{I_c(y)}{A_c} \right\} \tag{6}$$

where y denotes pixel indices within the patch-size $p_{15\times15}$. Here, ω denotes the predefined parameters and can be set to 0.95 according to [14].

Additionally, transmission maps produced with a patch-size of 3 × 3 are used to recover hazy background regions. To implement this transmission map $\tilde{t}_{p_{3\times3}}$, we compute

$$\tilde{t}_{p_{3\times3}}(x) = 1 - \omega \min_{y\in p_{3\times3}(x)} \left\{ \min_{c\in\{r,g,b\}} \frac{I_c(y)}{A_c} \right\} \tag{7}$$

where $p_{3\times3}$ represents a patch-size centered at a pixel index x, and y denotes a pixel index within the single patch-size $p_{3\times3}$. Moreover, a soft matting technique [35] is employed by which these two transmission maps $\tilde{t}_{p_{15\times15}}(x)$, $\tilde{t}_{p_{3\times3}}(x)$ can be refined as $t_{p_{15\times15}}(x)$, $t_{p_{3\times3}}(x)$ and thereby avoid the production of halo artifacts in the restored image.

Here, each region can be segmented by using the saliency maps of the hazy images [36]. However, the combination of two transmission maps via the saliency map by using the traditional fusion methods would suffer from generation of undesired artifacts (e.g., halo effects) along the edges of foreground objects [37]. Hence, the Laplacian-pyramids-based merging technique is used to reliably integrate these three maps into a hybrid transmission map for effective restoration of hazy images while avoiding undesired artifacts. Accordingly, the hybrid transmission map t_h can be represented as follows:

$$t_h(x) = \sum_{\mathcal{L}=\mathcal{L}_{\max}-1}^{1} \left(f^{\mathcal{L}}(x) + f^{\mathcal{L}+1}(x)\uparrow^{\mathcal{L}} \right) \tag{8}$$

where

$$\begin{aligned} f^{\mathcal{L}}(x) = {} & \left(S(x)\downarrow^{\mathcal{L}}\right) L^{\mathcal{L}}\left(t_{p_{15\times15}}(x)\right) \\ & + \left((1 - S(x))\downarrow^{\mathcal{L}}\right) L^{\mathcal{L}}\left(t_{p_{3\times3}}(x)\right) \end{aligned} \tag{9}$$

and $L^{\mathcal{L}}(\cdot)$ represents the processes of Laplacian pyramids [38]; $f^{\mathcal{L}}(x)$ represents the fused pyramids; $\mathcal{L}_{\max}$ denotes the number of pyramid levels and can be set to 5; $\uparrow$ and $\downarrow$ represent upsampling processing and downsampling processing, respectively. Note that S represents the binary saliency mask and can be acquired by using the method of Yang *et al.* according to [36].

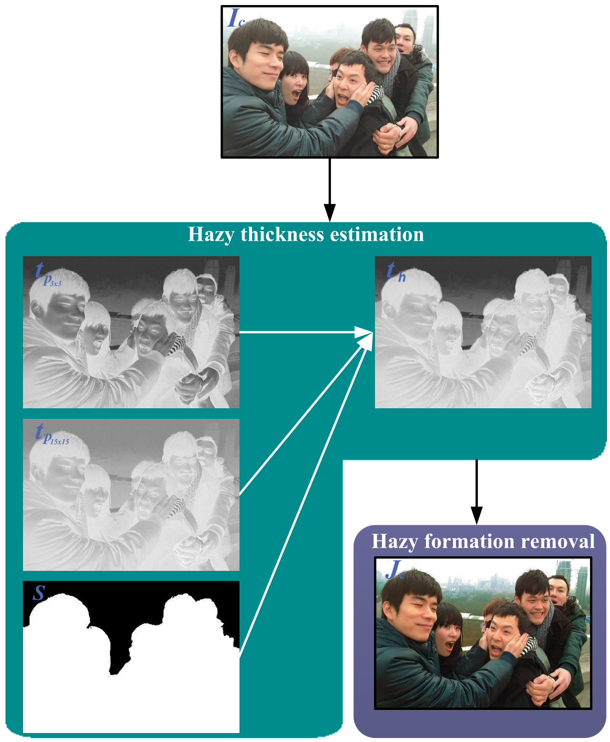

FIGURE 4. The flowchart of the proposed haze removal method.

B. HAZY FORMATION REMOVAL

After the hybrid transmission map t_h is generated during the proposed HTE module, the haze-free image J_c, which features both clear visibility restoration of background as well as complete maintenance of foreground objects, can be produced as follows:

$$J_c(x) = \frac{I_c(x) - A_c}{\max\{t_h(x), t_0\}} + A_c \tag{10}$$

where $I_c(x)$ represents the incoming hazy image, and t_0 is defined as 0.1 according to [14]. Note that the atmospheric lights A_c can be extracted from the corresponding region of the image $I_c(x)$ of the statistics of top 0.1% brightest pixels of the dark channel. As indicated previously, the flowchart of the proposed haze removal method is shown in Fig. 4.

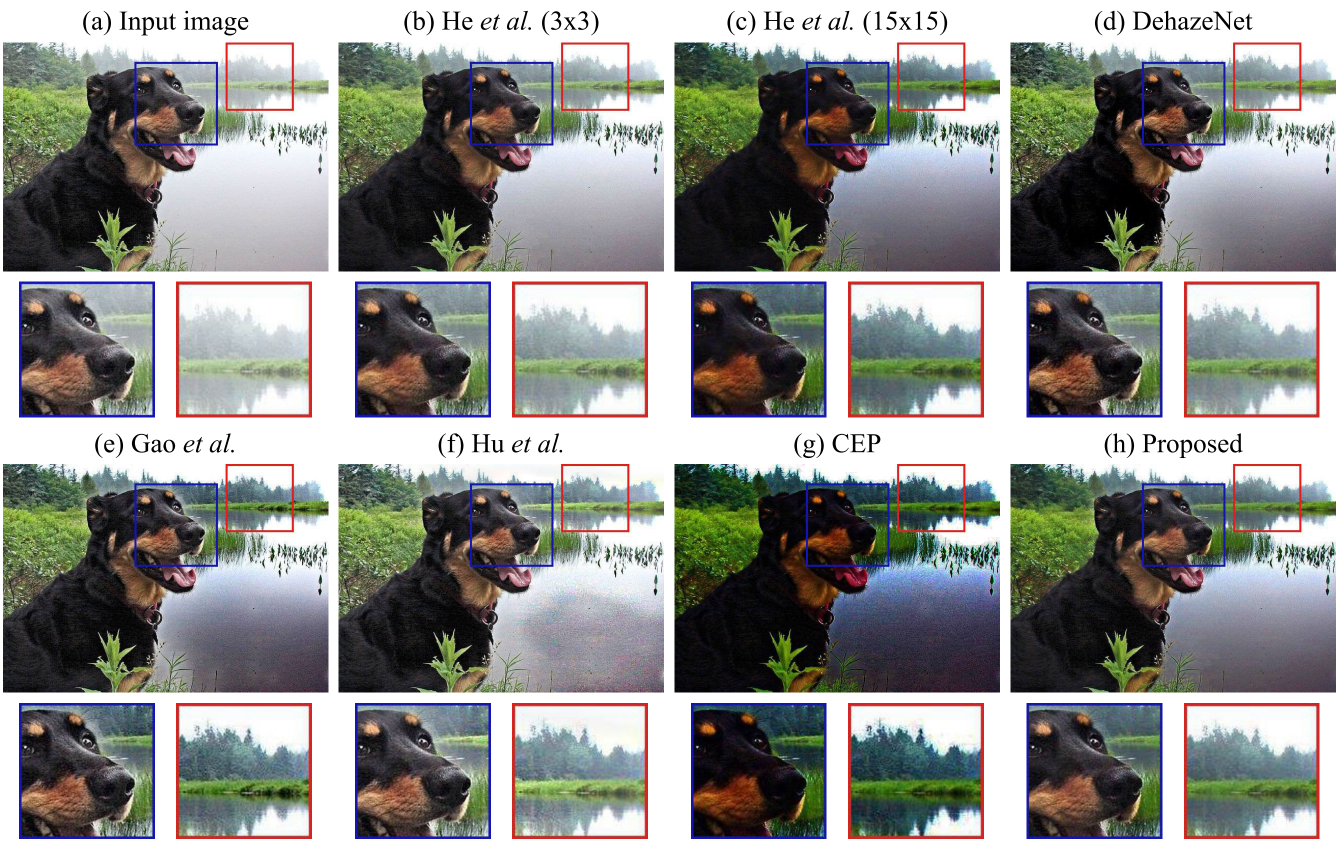

FIGURE 5. Image sampled from the "*Animal*" sequence: (a) input hazy image, with its corresponding foreground and background regions restored by the methods of (b) He *et al.* via a transmission map with a patch-size 3×3; (c) He *et al.* via the transmission map with a patch-size 15×15; (d) DehazeNet [16]; (e) Gao *et al.* [30]; (f) Hu *et al.* [31]; (g) CEP [21] and (h) the proposed method.

IV. EXPERIMENTAL RESULTS

In this section, we compare the performance of the proposed haze removal method with some of the other state-of-the-art methods [14], [16], [21], [30], [31]. These include the methods of He *et al.* [14] (which uses two patch-sizes: $p_{15\times15} = 15$ and $p_{3\times3} = 3$), Cai *et al.* [16] (learning-based dehaze algorithm, denoted as DehazeNet), Bui and Kim [21] (denoted as CEP), Gao *et al.* [30], and Hu *et al.* [31]. For these comparisons, we use qualitative and quantitative evaluations to assess restoration results generated via each haze removal method for hazy image sequences entitled "Animal," "People," and "Scene," as can be seen in Figs. 5-7 (a).

Here, we will demonstrate that the proposed method can achieve more effective restoration results for both background and foreground regions of hazy images than can the other state-of-the-art methods. To this end, in our comparisons, each test image is split into two sub-images according to the mean opinion score (MOS) of visual evaluations, which were performed by fifty experts in the image processing field, as well as fifty non-experts. The following subsections will present the quantitative and qualitative comparisons between each compared method in detail.

A. QUALITATIVE EVALUATIONS

In the first part, a visual assessment is conducted to evaluate the quality of restoration results. As shown in Figs. 5-7 (a), these hazy images contain disproportionate haze distribution consisting of a background region with heavy haze formation and a foreground region with little haze formation.

As shown in the red squares in Fig. 5 (b), it is apparent that the hazy image recovered by He *et al.*'s method often suffers from insufficient haze removal in the background region via the transmission maps generated with a patch-size 15×15. The use of patch-size 15×15 is well-suited for images containing proportionate haze distribution. In other words, images with proportionate haze distributions can be effectively restored by using the patch-size 15×15. However, when an image contains disproportionate haze distribution, the visibility of the background region within the image restored by adopting the patch-size 15×15 is less clear than that of an image restored by using the patch-size 3×3. This is because the use of patch-size 15×15 has a higher probability of extract the pixels of low intensity in the dark channel compared with the use of a patch-size 3×3. Such phenomena can also be observed in the two DCP-based methods as shown in Figs. 5-7 (b)-(c), (e)-(f), while they achieve fine results on the foreground but fail to recover the background. As for the DehazeNet method in Figs. 5-7 (d), it is evident that the hazy image recovered by the method cannot effectively achieve clear visibility restoration in the background region of the restored image. The main reason is that the neural network design of DehazeNet constitutes multiple large-size

FIGURE 6. Image sampled from the "*People*" sequence: (a) input hazy image, with its corresponding foreground and background regions restored by the methods of (b) He *et al.* via a transmission map with a patch-size 3 × 3; (c) He *et al.* via the transmission map with a patch-size 15 × 15; (d) DehazeNet [16]; (e) Gao *et al.* [30]; (f) Hu *et al.* [31]; (g) CEP [21] and (h) the proposed method.

FIGURE 7. Image sampled from the "*Scene*" sequence: (a) input hazy image, with its corresponding foreground and background regions restored by the methods of (b) He *et al.* via a transmission map with a patch-size 3 × 3; (c) He *et al.* via the transmission map with a patch-size 15 × 15; (d) DehazeNet [16]; (e) Gao *et al.* [30]; (f) Hu *et al.* [31]; (g) CEP [21] and (h) the proposed method.

pooling layers, thus it often generates smoothed transmission maps, and further result in failure removal of those haze in the background area. Despite the fine recovery on the background, the CEP method [21] overcompensate the foreground

TABLE 1. Qualitative evaluation results. The efficiency of the algorithm scores from 1 to 5, while higher score corresponding to better image quality.

Image Sequence	Proposed	DCP (p_{15})	DCP (p_3)	DehazeNet	CEP	Gao *et al.*	Hu *et al.*
Animal	4.18	2.21	3.17	3.31	1.64	4.01	3.98
People	3.92	2.13	3.06	3.24	1.51	3.88	3.73
Scene	3.51	2.08	3.11	3.18	1.57	3.47	3.44
Average	**3.81**	2.17	3.13	3.23	1.57	3.76	3.64

TABLE 2. Comparison of restoration rates attained by ***BRISQUE*** for a hazy image consisting of heavy haze formation within the background region and little haze formation within the foreground region.

Image Sequence	Proposed	DCP (p_{15})	DCP (p_3)	DehazeNet	CEP	Gao *et al.*	Hu *et al.*
Animal	38.351	38.331	36.531	37.644	45.691	43.035	44.322
People	46.474	46.476	46.213	46.281	47.045	46.476	47.074
Scene	39.261	39.466	41.491	37.776	39.613	37.500	39.833
Average	**40.4767**	41.0299	41.7998	40.9792	44.9049	42.6552	43.3487

as shown in Figs. 5-7 (g). In addition, as can be observed in the blue squares in Fig. 5 (b), the hazy image restored by He *et al.*'s method via the use of the transmission maps generated with a patch-size of 3×3 often results in excessive restoration of the foreground region. This is because the use of patch-size 3×3 has a low probability of finding low intensity pixels within the foreground region in the dark channel, thereby incorrectly regarding the foreground region as containing haze formation.

The qualitative evaluation results are shown in Table 1, while fifty experts in the image processing field as well as fifty non-experts were asked to score the algorithm based on two factors: the similarity of foreground region and haze-removal efficiency on the background region before/after applying each haze removal algorithm. As shown in the table, the proposed method obtain the highest overall MOS among other state-of-the-art algorithms. We employ the proposed HTE module by which to generate a hybrid transmission map. Because of this, the proposed approach can effectively produce a satisfactory restored image that features both clear visibility restoration and effective structure maintenance due to use of the proposed HFR module, as shown in the blue and red squares in Figs. 5-7 (h). Based on the restoration results and the qualitative evaluation, the proposed method attains more effective restoration results than the methods of He *et al.* [14], DehazeNet [16], CEP [21], Gao *et al.* [30], and Hu *et al.* [31].

B. QUANTITATIVE EVALUATIONS

The purpose of this part of our paper is to demonstrate via quantitative evaluations that the proposed method can attain effective restoration results for hazy images containing disproportionate haze distributions.

In general, the objective metrics used for the quantitative evaluations can be grouped into two types: reference image approaches and non-reference image approaches. The reference image evaluation approaches can be accomplished through the use of both a real-world haze-free reference image and an incoming hazy image. Since there is no real-world haze-free background reference image, the reference image approach cannot be used for assessing the background regions of our test images. Therefore, in order to accomplish an objective comparison, we employ the non-reference image quality assessment approach to evaluate the background regions. The *BRISQUE* method proposed by Mittal *et al.* [39], which belongs to the non-reference image approach category, is adopted for assessing the level of contrast restoration between the image after and before haze removal. Note that a lower value of *BRISQUE* represents more effective recovery results in the restored image. The quantitative evaluation results of each method are listed in Table 2.

As demonstrated by Table 2, it is apparent that the proposed method outperforms these DCP-based methods [14], [30], [31], and other state-of-the-art haze removal methods [16], [21]. This is due to the proposed haze removal method's ability to effectively generate a high-quality image that exhibits clear visibility restoration for the background region while intrinsically maintaining the structure of the foreground region.

From both qualitative and quantitative evaluations, we can clearly observe that the proposed haze removal method can provide more effective restoration results than can the other dark channel prior-based methods [14], [30], [31], the CEP method [21] and learning-based DehazeNet [16] method. This is because the proposed method integrates the advantages of two transmission maps produced by using the patch-sizes 15×15 and 3×3 to produce a hybrid transmission map and thereby attain a high-quality restored image that offers both clear visibility restoration of the background region and effective maintenance of the intrinsic structure information of the foreground region.

V. CONCLUSION

In this paper, we propose a novel haze removal method constructed by the proposed HTE module and the proposed HFR module to effectively attain clear visibility restoration for background regions of hazy images while simultaneously maintaining the intrinsic structure information of foreground regions. In the proposed HTE module, we use a Laplacian-pyramids-based merging technique by which to generate a hybrid transmission map by integrating the advantages of two transmission maps produced by using patch-sizes 15×15 and 3×3. After the proposed HTE module is performed, the proposed HFR module adopts the hybrid transmission map to restore the hazy image, resulting in both clear visibility restoration in the background region and effective intrinsic structure maintenance of the foreground region. Experimental results suggest that our proposed method attains more effective restoration of a hazy image than the other state-of-the-art methods in both background and foreground regions. Both quantitative and qualitative comparisons support this claim; for instance, the proposed method simultaneously achieves the best *BRISQUE* and MOS comparing with existing approaches.

REFERENCES

[1] S.-C. Huang and B.-H. Chen, "Automatic moving object extraction through a real-world variable-bandwidth network for traffic monitoring systems," *IEEE Trans. Ind. Electron.*, vol. 61, no. 4, pp. 2099–2112, Apr. 2014.

[2] S.-C. Huang, "An advanced motion detection algorithm with video quality analysis for video surveillance systems," *IEEE Trans. Circuits Syst. Video Technol.*, vol. 21, no. 1, pp. 1–14, Jan. 2011.

[3] S.-C. Huang and B.-H. Do, "Radial basis function based neural network for motion detection in dynamic scenes," *IEEE Trans. Cybern.*, vol. 44, no. 1, pp. 114–125, Jan. 2014.

[4] S.-C. Huang, D.-W. Jaw, B.-H. Chen, and S.-Y. Kuo, "An efficient single image enhancement approach using luminance perception transformation," *IEEE Trans. Emerg. Topics Comput.*, early access, Sep. 25, 2019, doi: 10.1109/TETC.2019.2943231.

[5] S.-C. Huang, T.-H. Le, and D.-W. Jaw, "DSNet: Joint semantic learning for object detection in inclement weather conditions," *IEEE Trans. Pattern Anal. Mach. Intell.*, early access, Mar. 3, 2020, doi: 10.1109/TPAMI.2020.2977911.

[6] K. Zheng, H. Meng, P. Chatzimisios, L. Lei, and X. Shen, "An SMDP-based resource allocation in vehicular cloud computing systems," *IEEE Trans. Ind. Electron.*, vol. 62, no. 12, pp. 7920–7928, Dec. 2015.

[7] S.-C. Huang, M.-K. Jiau, and C.-A. Hsu, "A high-efficiency and high-accuracy fully automatic collaborative face annotation system for distributed online social networks," *IEEE Trans. Circuits Syst. Video Technol.*, vol. 24, no. 10, pp. 1800–1813, Oct. 2014.

[8] Y. Y. Schechner, S. G. Narasimhan, and S. K. Nayar, "Polarization-based vision through haze," *Appl. Opt.*, vol. 42, no. 3, pp. 511–525, Jan. 2003. [Online]. Available: http://ao.osa.org/abstract.cfm?URI=ao-42-3-511

[9] S. G. Narasimhan and S. K. Nayar, "Contrast restoration of weather degraded images," *IEEE Trans. Pattern Anal. Mach. Intell.*, vol. 25, no. 6, pp. 713–724, Jun. 2003.

[10] S. K. Nayar and S. G. Narasimhan, "Vision in bad weather," in *Proc. 7th IEEE Int. Conf. Comput. Vis.*, vol. 2, 1999, pp. 820–827.

[11] S. G. Narasimhan and S. Nayar, "Interactive (de) weathering of an image using physical models," in *Proc. IEEE Workshop Color Photometric Methods Comput. Vis.*, Oct. 2003, p. 1.

[12] J. Kopf, B. Neubert, B. Chen, M. Cohen, D. Cohen-Or, O. Deussen, M. Uyttendaele, and D. Lischinski, "Deep photo: Model-based photograph enhancement and viewing," *ACM Trans. Graph.*, vol. 27, no. 5, p. 116, Dec. 2008. [Online]. Available: http://doi.acm.org/10.1145/1409060.1409069

[13] K. Tan and J. P. Oakley, "Enhancement of color images in poor visibility conditions," in *Proc. Int. Conf. Image Process.*, vol. 2, Sep. 2000, pp. 788–791.

[14] K. He, J. Sun, and X. Tang, "Single image haze removal using dark channel prior," *IEEE Trans. Pattern Anal. Mach. Intell.*, vol. 33, no. 12, pp. 2341–2353, Dec. 2011.

[15] D. Berman, T. Treibitz, and S. Avidan, "Non-local image dehazing," in *Proc. IEEE Conf. Comput. Vis. Pattern Recognit. (CVPR)*, Jun. 2016, pp. 1674–1682.

[16] B. Cai, X. Xu, K. Jia, C. Qing, and D. Tao, "DehazeNet: An end-to-end system for single image haze removal," *IEEE Trans. Image Process.*, vol. 25, no. 11, pp. 5187–5198, Nov. 2016.

[17] W. Ren, S. Liu, H. Zhang, J. Pan, X. Cao, and M.-H. Yang, "Single image dehazing via multi-scale convolutional neural networks," in *Proc. Eur. Conf. Comput. Vis. (ECCV)*. Amsterdam, The Netherlands: Springer, 2016, pp. 154–169.

[18] B. Li, X. Peng, Z. Wang, J. Xu, and D. Feng, "AOD-net: All-in-one dehazing network," in *Proc. IEEE Int. Conf. Comput. Vis. (ICCV)*, Oct. 2017, pp. 4780–4788.

[19] B.-H. Chen, S.-C. Huang, C.-Y. Li, and S.-Y. Kuo, "Haze removal using radial basis function networks for visibility restoration applications," *IEEE Trans. Neural Netw. Learn. Syst.*, vol. 29, no. 8, pp. 3828–3838, Aug. 2018.

[20] W. Ren, L. Ma, J. Zhang, J. Pan, X. Cao, W. Liu, and M.-H. Yang, "Gated fusion network for single image dehazing," in *Proc. IEEE/CVF Conf. Comput. Vis. Pattern Recognit.*, Jun. 2018, pp. 3253–3261.

[21] T. M. Bui and W. Kim, "Single image dehazing using color ellipsoid prior," *IEEE Trans. Image Process.*, vol. 27, no. 2, pp. 999–1009, Feb. 2018.

[22] S. Huang, D. Li, W. Zhao, and Y. Liu, "Haze removal algorithm for optical remote sensing image based on multi-scale model and histogram characteristic," *IEEE Access*, vol. 7, pp. 104179–104196, 2019.

[23] C. Wang, Z. Li, J. Wu, H. Fan, G. Xiao, and H. Zhang, "Deep residual haze network for image dehazing and deraining," *IEEE Access*, vol. 8, pp. 9488–9500, 2020.

[24] H. Zhang and V. M. Patel, "Densely connected pyramid dehazing network," in *Proc. IEEE/CVF Conf. Comput. Vis. Pattern Recognit.*, Jun. 2018, pp. 3194–3203.

[25] R. Fattal, "Single image dehazing," *ACM Trans. Graph.*, vol. 27, no. 3, p. 72, Aug. 2008. [Online]. Available: http://doi.acm.org/10.1145/1360612.1360671

[26] R. T. Tan, "Visibility in bad weather from a single image," in *Proc. IEEE Conf. Comput. Vis. Pattern Recognit.*, Jun. 2008, pp. 1–8.

[27] Y. Wang and B. Wu, "Improved single image dehazing using dark channel prior," in *Proc. IEEE Conf. Intell. Comput. Intell. Syst.*, vol. 2, Oct. 2010, pp. 789–792.

[28] E. Ullah, R. Nawaz, and J. Iqbal, "Single image haze removal using improved dark channel prior," in *Proc. 5th Int. Conf. Modelling, Identificat. Control (ICMIC)*, Aug./Sep. 2013, pp. 245–248.

[29] H. Xu, J. Guo, Q. Liu, and L. Ye, "Fast image dehazing using improved dark channel prior," in *Proc. IEEE Int. Conf. Inf. Sci. Technol.*, Mar. 2012, pp. 663–667.

[30] Y. Gao, H.-M. Hu, B. Li, Q. Guo, and S. Pu, "Detail preserved single image dehazing algorithm based on airlight refinement," *IEEE Trans. Multimedia*, vol. 21, no. 2, pp. 351–362, Feb. 2019.

[31] H.-M. Hu, H. Zhang, Z. Zhao, B. Li, and J. Zheng, "Adaptive single image dehazing using joint local-global illumination adjustment," *IEEE Trans. Multimedia*, vol. 22, no. 6, pp. 1485–1495, Jun. 2020.

[32] J. Y. Chiang and Y.-C. Chen, "Underwater image enhancement by wavelength compensation and dehazing," *IEEE Trans. Image Process.*, vol. 21, no. 4, pp. 1756–1769, Apr. 2012.

[33] Y.-H. Shiau, H.-Y. Yang, P.-Y. Chen, and Y.-Z. Chuang, "Hardware implementation of a fast and efficient haze removal method," *IEEE Trans. Circuits Syst. Video Technol.*, vol. 23, no. 8, pp. 1369–1374, Aug. 2013.

[34] S.-C. Huang, B.-H. Chen, and W.-J. Wang, "Visibility restoration of single hazy images captured in real-world weather conditions," *IEEE Trans. Circuits Syst. Video Technol.*, vol. 24, no. 10, pp. 1814–1824, Oct. 2014.

[35] A. Levin, D. Lischinski, and Y. Weiss, "A closed-form solution to natural image matting," *IEEE Trans. Pattern Anal. Mach. Intell.*, vol. 30, no. 2, pp. 228–242, Feb. 2008.

[36] C. Yang, L. Zhang, H. Lu, X. Ruan, and M.-H. Yang, "Saliency detection via graph-based manifold ranking," in *Proc. IEEE Conf. Comput. Vis. Pattern Recognit.*, Jun. 2013, pp. 3166–3173.

[37] C. Thomas, T. Ranchin, L. Wald, and J. Chanussot, "Synthesis of multispectral images to high spatial resolution: A critical review of fusion methods based on remote sensing physics," *IEEE Trans. Geosci. Remote Sens.*, vol. 46, no. 5, pp. 1301–1312, May 2008.

[38] P. Burt and E. Adelson, "The Laplacian pyramid as a compact image code," *IEEE Trans. Commun.*, vol. 31, no. 4, pp. 532–540, Apr. 1983.

[39] A. Mittal, A. K. Moorthy, and A. C. Bovik, "Blind/Referenceless image spatial quality evaluator," in *Proc. Conf. Rec. 45th Asilomar Conf. Signals, Syst. Comput. (ASILOMAR)*, Nov. 2011, pp. 723–727.

SHIH-CHIA HUANG (Senior Member, IEEE) received the B.S. degree from National Taiwan Normal University, Taipei, Taiwan, the M.S. degree from National Chiao Tung University, Hsinchu, Taiwan, and the Ph.D. degree in electrical engineering from National Taiwan University, Taipei, in 2009. He is currently a Full Professor with the Department of Electronic Engineering, National Taipei University of Technology, Taipei, and an International Adjunct Professor with the Faculty of Business and Information Technology, University of Ontario Institute of Technology, Oshawa, ON, Canada. He has authored and coauthored more than 100 journal and conference papers and holds more than 60 patents in the U.S., Europe, Taiwan, and China. His research interests include intelligent multimedia systems, image processing and video coding, video surveillance systems, cloud computing and big data analytics, artificial intelligence, and mobile applications and systems. He was a recipient of the Kwoh-Ting Li Young Researcher Award in 2011 from the Taipei Chapter of the Association for Computing Machinery; the 5th National Industrial Innovation Award in 2017 from the Ministry of Economic Affairs, Taiwan; the Dr. Shechtman Young Researcher Award in 2012 from the National Taipei University of Technology; the Outstanding Research Award from the National Taipei University of Technology in 2014 and 2017; and the College of Electrical Engineering and Computer Science, National Taipei University of Technology in 2014 to 2016. He is also the Chapter Chair of the IEEE Taipei Section Broadcast Technology Society. He is also the Services and Applications Track Chair of IEEE CloudCom 2016–2017 Conference, the Applications Track Chair of the IEEE BigData Congress in 2015, the General Chair of the 2015–2016 IEEE BigData Taipei Satellite Session, and the Deep Learning, Ubiquitous and Toy Computing Minitrack Chair. He was an Associate Editor of the *Journal of Artificial Intelligence* and a Guest Editor of the *Engineering Applications of Artificial Intelligence*, the *Information Systems Frontiers* and the *International Journal of Web Services Research*. He is also an Associate Editor of the IEEE SENSORS JOURNAL and *Electronic Commerce Research and Applications*.

DA-WEI JAW received the B.S. and M.S. degrees in electronic engineering from the National Taipei University of Technology, Taipei, Taiwan, in 2015 and 2017, respectively. He is currently pursuing the Ph.D. degree in electrical engineering with National Taiwan University. His research interests include digital image processing, machine learning, and neural networks.

WENLI LI received the master's degree in educational technology from East China Normal University, in 2003. She is currently an Associate Professor with Shenzhen Polytechnic. Her research interests include service computing technology and information teaching. She is also an Executive Director of the National CBE Society and the Guangdong Provincial Committee of Education and Technology in Colleges and Universities.

ZHIHUI LU (Member, IEEE) received the Ph.D. degree in computer science from Fudan University, in 2004. He is currently a Professor with the School of Computer Science, Fudan University. His research interests include big data architecture, cloud computing and service computing technology, edge computing, smart city, and the IoT. He is also a member of the China Computer Federation's Service Computing Specialized Committee.

SY-YEN KUO (Fellow, IEEE) received the B.S. degree in electrical engineering from National Taiwan University, Taipei, in 1979, the M.S. degree in electrical and computer engineering from the University of California at Santa Barbara, Santa Barbara, CA, USA, in 1982, and the Ph.D. degree in computer science from the University of Illinois at Urbana-Champaign, Champaign, IL, USA, in 1987. From 1982 to 1984, he was an Engineer with Fairchild Semiconductor, Sunnyvale, CA, USA, and Silvar-Lisco, Menlo Park, CA, USA. From 1988 to 1991, he was a Faculty Member with the Department of Electrical and Computer Engineering, The University of Arizona. In 1989, he also worked as a Summer Faculty Fellow with the Jet Propulsion Laboratory, California Institute of Technology. From 2001 to 2004, he was the Chairman of the Department of Electrical Engineering, National Taiwan University (NTU), Taipei, where he was also the Dean of the College of Electrical Engineering and Computer Science, from 2012 to 2015. He also took a leave from NTU and served as the Chair Professor and the Dean for the College of Electrical Engineering and Computer Science, National Taiwan University of Science and Technology, from 2006 to 2009. He spent his sabbatical years as a Visiting Professor with The Hong Kong Polytechnic University, from 2011 to 2012, and with The Chinese University of Hong Kong, from 2004 to 2005, and as a Visiting Researcher with the AT&T Labs-Research, Middletown, NJ, USA, from 1999 to 2000. He is currently the Pegatron Chair Professor with the Department of Electrical Engineering, NTU. He has authored or coauthored more than 400 papers in journals and conferences, and holds 21 U.S. patents, 19 Taiwan patents, and ten patents from other countries. His current research interests include dependable systems and networks, mobile computing, cloud computing, and quantum computing and communications. He was a recipient of the Best Paper Award in the 1996 International Symposium on Software Reliability Engineering, the Best Paper Award in the Simulation and Test Category at the 1986 IEEE/ACM Design Automation Conference, the National Science Foundation's Research Initiation Award in 1989, the IEEE/ACM Design Automation Scholarship in 1990 and 1991, and the Distinguished Research Award and the Distinguished Research Fellow Award from the National Science Council, Taiwan.

BENJAMIN C. M. FUNG (Senior Member, IEEE) received the Ph.D. degree in computing science from Simon Fraser University, Canada, in 2007. He is currently a Professor with the School of Information Studies, McGill University, Canada. He is also a licensed Professional Engineer of software engineering in Canada. He has over 120 refereed publications that span the research forums of data mining, privacy protection, cybersecurity, services computing, and building engineering. He is also the Canada Research Chair in data mining for cybersecurity and a Co-Curator of cybersecurity with World Economic Forum. He also serves as an Associate Editor for IEEE Transactions of Knowledge and Data Engineering and *Sustainable Cities and Society (SCS)* (Elsevier).

BO-HAO CHEN (Member, IEEE) received the Ph.D. degree in electronic engineering from the National Taipei University of Technology, Taipei, in 2014. He is currently an Assistant Professor with the Department of Computer Science and Engineering, Yuan Ze University, Taoyuan, Taiwan. His current research interests include digital image processing, video coding, multimedia big data computing, and content analysis and mining of multimedia big data. He was a recipient for Involvement in Research with the Department of Cybernetics, Tula State University, Tula, Russia, in 2014. He received the Best Student Paper Award from the IEEE International Symposium on Multimedia in 2013, the Best Paper Award from the ACM International Conference on Big Data and Advanced Wireless Technologies in 2016, the First Paper Award from the IEEE International Conference on Applied System Innovation in 2017, and the Best Ph.D. Dissertation Award from the IEEE Taipei Section and the Taiwan Institute of Electrical and Electronic Engineering in 2014.

THANISA NUMNONDA received the Ph.D. degree in computer science from the National Institute of Development Administration, Thailand, in 2012. She has been a Lecturer with the Faculty of Information Technology, King Mongkut's Institute of Technology Ladkrabang, Thailand, since May 2005, and became an Associate Professor since June 2006. In August 2019, she decided to join IMC Institute full time.